Pharm Res (2015) 32:941–954
DOI 10.1007/s11095-014-1508-y

RESEARCH PAPER

# Laronidase-Functionalized Multiple-Wall Lipid-Core Nanocapsules: Promising Formulation for a More Effective Treatment of Mucopolysaccharidosis Type I

Fabiana Quoos Mayer • Márcia Duarte Adorne • Eduardo André Bender • Talita Giacomet de Carvalho • Anna Cláudia Dilda • Ruy Carlos Ruver Beck • Sílvia Stanisçuaski Guterres • Roberto Giugliani • Ursula Matte • Adriana Raffin Pohlmann

Received: 17 May 2014 / Accepted: 29 August 2014 / Published online: 11 September 2014


## ABSTRACT

***Purpose*** Mucopolysaccharidosis I is a genetic disorder caused by alpha-L-iduronidase deficiency. Its primary treatment is enzyme replacement therapy (ERT), which has limitations such as a high cost and a need for repeated infusions over the patient's lifetime. Considering that nanotechnological approaches may enhance enzyme delivery to organs and can reduce the dosage thereby enhancing ERT efficiency and/or reducing its cost, we synthesized laronidase surface-functionalized lipid-core nanocapsules (L-MLNC).

***Methods*** L-MLNCs were synthesized by using a metal complex. Size distributions were evaluated by laser diffraction and dynamic light scattering. The kinetic properties, cytotoxicity, cell uptake mechanisms, clearance profile and biodistribution were evaluated.

***Results*** Size distributions showed a D[4,3] of 134 nm and a z-average diameter of 71 nm. L-MLNC enhanced the Vmax and Kcat in comparison with laronidase. L-MLNC is not cytotoxic, and nanocapsule uptake by active transport is not only mediated by mannose-6-phosphate receptors. The clearance profile is better for L-MLNC than for laronidase. A biodistribution analysis showed enhanced enzyme activity in different organs within 4 h and 24 h for L-MLNC.

***Conclusions*** The use of lipid-core nanocapsules as building blocks to synthesize surface-functionalized nanocapsules represents a new platform for producing decorated soft nanoparticles that are able to modify drug biodistribution.

**KEY WORDS** enzyme replacement therapy · laronidase · mucopolysaccharidosis I · multiple-wall lipid-core nanocapsules · surface functionalization

Fabiana Quoos Mayer and Márcia Duarte Adorne contributed equally to this study

**Electronic supplementary material** The online version of this article (doi:10.1007/s11095-014-1508-y) contains supplementary material, which is available to authorized users.

F. Q. Mayer • T. G. de Carvalho • A. C. Dilda • R. Giugliani • U. Matte
Gene Therapy Center, Experimental Research Center Hospital de Clínicas de Porto Alegre Porto Alegre RS, Brazil

F. Q. Mayer • T. G. de Carvalho • R. Giugliani • U. Matte (✉)
Post-Graduation Program on Genetics and Molecular Biology Universidade Federal do Rio Grande do Sul Porto Alegre RS, Brazil
e-mail: umatte@hcpa.ufrgs.br

M. D. Adorne • E. A. Bender • R. C. R. Beck • S. S. Guterres • A. R. Pohlmann
Programa de Pós-Graduação em Ciências Farmacêuticas, Faculdade de Farmácia Universidade Federal do Rio Grande do Sul Porto Alegre RS, Brazil

R. Giugliani
Medical Genetics Service, HCPA, and Department of Genetics/UFRGS Porto Alegre RS, Brazil

A. R. Pohlmann (✉)
Departamento de Química Orgânica, Instituto de Química Universidade Federal do Rio Grande do Sul Porto Alegre RS, Brazil
e-mail: adriana.pohlmann@ufrgs.br

*Present Address:*
F. Q. Mayer
Instituto de Pesquisas Veterinárias Desidério Finamor Fundação Estadual de Pesquisa Agropecuária Eldorado do Sul RS, Brazil

## ABBREVIATIONS

| | |
|---|---|
| BS | Backscattering |
| CNS | Central Nervous System |
| ERT | Enzyme Replacement Therapy |
| IDUA | Alpha-L-iduronidase |
| $L_1$-MLNC$_1$ | Multiple-wall nanocapsule with 0.05% chitosan and 11 $\mu$g/mL of laronidase |
| $L_1$-MLNC$_2$ | Multiple-wall nanocapsule with 0.075% chitosan and 11 $\mu$g/mL of laronidase |
| $L_2$-MLNC$_1$ | Multiple-wall nanocapsule with 0.05% chitosan and 96 $\mu$g/mL of laronidase |
| $L_2$-MLNC$_2$ | Multiple-wall nanocapsule with 0.075% chitosan and 96 $\mu$g/mL of laronidase |
| L-MLNC | Laronidase surface-functionalized lipid-core nanocapsules |
| LNC | Lipid core nanocapsules |
| LNC-CS$_{0.03}$ | LNC coated with 0.03% (*w/v*) chitosan |
| LNC-CS$_{0.05}$ | LNC coated with 0.05% (*w/v*) chitosan |
| LNC-CS$_{0.075}$ | LNC coated with 0.075% (*w/v*) chitosan |
| MPS I | Mucopolysaccharidosis type I |
| MTT | 3-(4,5-dimethylthiazol-2-yl)-2,5-diphenyl tetrazolium bromide |
| PCS | Photon Correlation Spectroscopy |
| PDI | Polydispersity Index |
| T | Transmission |
| ΔBS | Relative Backscattering |

## INTRODUCTION

Advances in genetic engineering and biotechnology have enabled the identification of a range of peptides and proteins that are potentially useful for preventing or reversing disease processes (1,2). These proteins are organic products with relatively high specificity and, thus, low doses can produce therapeutic effects. However, the application of these biomolecules is impaired by their low bioavailability and high clearance rate through enzymatic degradation (1). Thus, the use of nanotechnology to deliver enzymes could be a promising strategy for increasing therapeutic efficacy.

Drug targeting with nanoparticles causes an increase in the drug concentration at the site of action relative to pure drug administration because of encapsulation, a strategy that serves to mask the physico-chemical characteristics of the drug. Different nanoencapsulation mechanisms can be achieved by combining the physico-chemical characteristics of the drug with the nanocarrier as follows: i) retention or dissolution within a soft colloid, ii) sorption on the colloid surface by electrostatic interactions, and iii) chemical conjugation with a colloid material. The goal of targeting using nanoencapsulation is to improve the pharmacological response to drugs by increasing the drug absorption (2) and/or apparent solubility in aqueous media by controlling the drug delivery (3) in addition to modifying the drug biodistribution and pharmacokinetics (4). Additionally, the drug can be directed to tissues that are difficult to access because of biological barriers, such as the blood brain barrier (5). Moreover, because drug properties are masked by nanoencapsulation, the dose of the drug to be administered can be reduced, thus avoiding a major problem associated with the systemic administration of a free drug and its non-selective biodistribution in the body. This lack of selectivity can require high drug doses to achieve therapeutic concentrations at the site of action, leading to increased drug toxicity (3). The conjugation of proteins on nanoparticles, such as several types of antibodies, hormones and enzymes, is a promising strategy for drug targeting and for protecting against degradation or rapid capture by the immune system (6). These biomolecules can be covalently bound to the nanoparticle surface by using cross-linker molecules to minimize non-specific interactions and also to avoid protein denaturation or a loss of activity by steric hindrance (7). Although it is an attractive strategy for promoting a stable bond between proteins and nanocarriers, covalent binding has drawbacks because of its complexity, multiple step synthesis and the possible occurrence of secondary reactions during the conjugation process (6,8).

We previously developed new biodegradable nanocarriers known as lipid-core nanocapsules (9,10), which are composed of an organogel as the core, a polymeric wall and polysorbate 80 micelles as the external coating. The lipid-core nanocapsules are formed by self-assembly, the mechanism of which was recently determined (11). This nanocapsule has shown diverse deformation properties when compared with conventional polymeric nanocapsules (12), and it is more rigid than the conventional nanocapsules according to atomic force microscopy. Drug-loaded lipid-core nanocapsules are potential formulations for treating inflammation (13,14), multiform glioblastoma (15) and myeloid leukemia (16). For the first time, brain drug targeting has been demonstrated after the oral administration of resveratrol-loaded lipid-core nanocapsules in rats (17). Considering the ability of the lipid-core nanocapsules to cross certain biological barriers, such as oral absorption and the blood-brain barrier, in addition to their physico-chemical colloidal stability (10) and hemocompatibility (18), we proposed the use of these nanocapsules as building blocks for the functionalization of the surface with enzymes using a chitosan-metal complex as an innovative strategy for surface decoration (19). This strategy also considered the feasibility of chitosan-metal complexes

to adsorb drugs with heteroatoms in their chemical structure, such as oxygen or nitrogen, as previously reported for microparticles (20).

We therefore used Mucopolysaccharidosis type I (MPS I, OMIM #607014), a lysosomal storage disorder which is caused by α-L-iduronidase (IDUA; EC 3.2.1.76) deficiency as a model for application of enzyme functionalized nanocapsules. The α-L-iduronidase cleaves α-L-iduronic and L- iduronic acid residues from the glycosaminoglycans dermatan and heparan sulfate (21), and thus the enzyme deficiency leads to the systemic accumulation of these substances. The treatment of choice for MPS I is enzyme replacement therapy (ERT), in which a recombinant enzyme is administered to the patient every two weeks. This therapy has the following limitations: i) the neurological symptoms are not corrected because the enzyme does not cross the blood brain barrier (22), ii) high cost (usually over US$ 100,000/patient per year) (23), and iii) the immunological response to the infused enzyme frequently necessitates the administration of antipyretics and/or antihistamines before enzyme infusion (24).

The efficacy of ERT for MPS I may benefit from nanotechnology-based modifications, enhancing enzyme delivery to organs and possibly allowing a dose reduction, which may represent either a decrease in the adverse events observed in patients or a decrease in the cost of the therapy. Targeting the IDUA in a nanoparticle may help to improve ERT, because a more effective device could alter the pharmacokinetic and biodistribution profiles. Thus, we propose the synthesis of an innovative nanocapsule that is functionalized with laronidase to improve the enzyme activity. The new carrier formed by a biocompatible and biodegradable polysaccharide-metal complex would be capable of binding different molecular or macromolecular species on the nanocapsule surface. The supramolecular structure of this new nanocarrier is built by coating the lipid-core nanocapsules layer-by-layer with a negative surface, which is in turn coated with chitosan (a polycationic macromolecule), followed by the addition of iron as a metal that is used as a specific chemisorption site for laronidase, the commercially available enzyme for MPS I treatment. The new nanocarriers were called laronidase-functionalized multiple-wall lipid-core nanocapsules (L-MLNC), and they have a supramolecular architecture as presented in Fig. 1. *In vitro* and *in vivo* biological assays were conducted to evaluate our hypothesis.

## MATERIALS AND METHODS

### Ethical Issues

The Ethics Research Committee of the Hospital de Clínicas de Porto Alegre (HCPA) approved this study (GPPG 09-334 and GPPG 11-0302). An MPS I patient's fibroblasts were obtained from the Medical Genetics Service of HCPA under informed consent. *Idua* knockout mice (*Idua*$^{-/-}$; C57BL/6 background) were kindly provided by Dr. Elizabeth Neufeld (UCLA, USA) and were maintained at the Experimental Animal Unit from HCPA under 12 h dark/light cycles with food and water ad libitum.

### Preparing Laronidase-Functionalized Multiple-Wall Lipid Core Nanocapsules

Lipid core nanocapsules (LNC) were used as building blocks for the multiple-wall nanocapsules. LNC suspensions were prepared as previously reported by the interfacial deposition of preformed polymer (10,18). An organic phase containing poli(ε-caprolactone) (PCL) (MW = 14,000 g mol$^{-1}$, Aldrich, France), Span 60 (sorbitan monostearate) (Aldrich, France) and capric and caprylic triglyceride (Delaware, Brazil) were prepared with acetone at 40°C. Lipoid® S75 (75% in phosphatidylcholine, Gerbras, Brazil) was dissolved in ethanol and added to the organic phase. The aqueous phase was prepared by dispersing polysorbate 80 (Delaware, Brazil) in water. The organic phase was injected continuously into the aqueous solution. After 10 min, the organic solvent was removed and the suspension was concentrated under reduced pressure to adjust the final volume to 10 mL. To coat the LNC with chitosan, a 0.3% (*w*/*v*) chitosan solution (low molecular weight chitosan (CS) with a deacetylation degree of 75.6%, and a viscosity of 20,000 CPS; Aldrich, France) was prepared in acetic acid 1% (*v*/*v*) and filtered. To determine the best chitosan concentration, three different amounts of chitosan solution were used to produce final chitosan concentrations of 0.03%, 0.05% and 0.075% (*w*/*v*) for LNC-$CS_{0.03}$, LNC-$CS_{0.05}$ and LNC-$CS_{0.075}$, respectively. After the coating step, a 0.018 mol L$^{-1}$ $Fe^{2+}$ solution was prepared from $FeCl_2.H_2O$ (Aldrich, USA), and ultrapure water was added to each chitosan-coated lipid-core nanocapsule suspension under high magnetic stirring. The final iron concentration in the formulations was 4.5 mmol L$^{-1}$. After 1 min of $Fe^{2+}$ addition, 11 μg mL$^{-1}$ or 96 μg mL$^{-1}$ of laronidase (Aldurazyme®, Genzyme Corporation, Cambridge, USA) was added to the formulations to obtain the laronidase-functionalized multiple-wall lipid-core nanocapsules (L-MLNC).

### The Physicochemical Characterization of the Formulations

The formulations were characterized before and after coating with chitosan and functionalizing with the enzyme. All experiments were performed using three different batches of each formulation.

The granulometric profiles were determined by a Mastersizer 2000 (Malvern Instruments, UK) after injecting

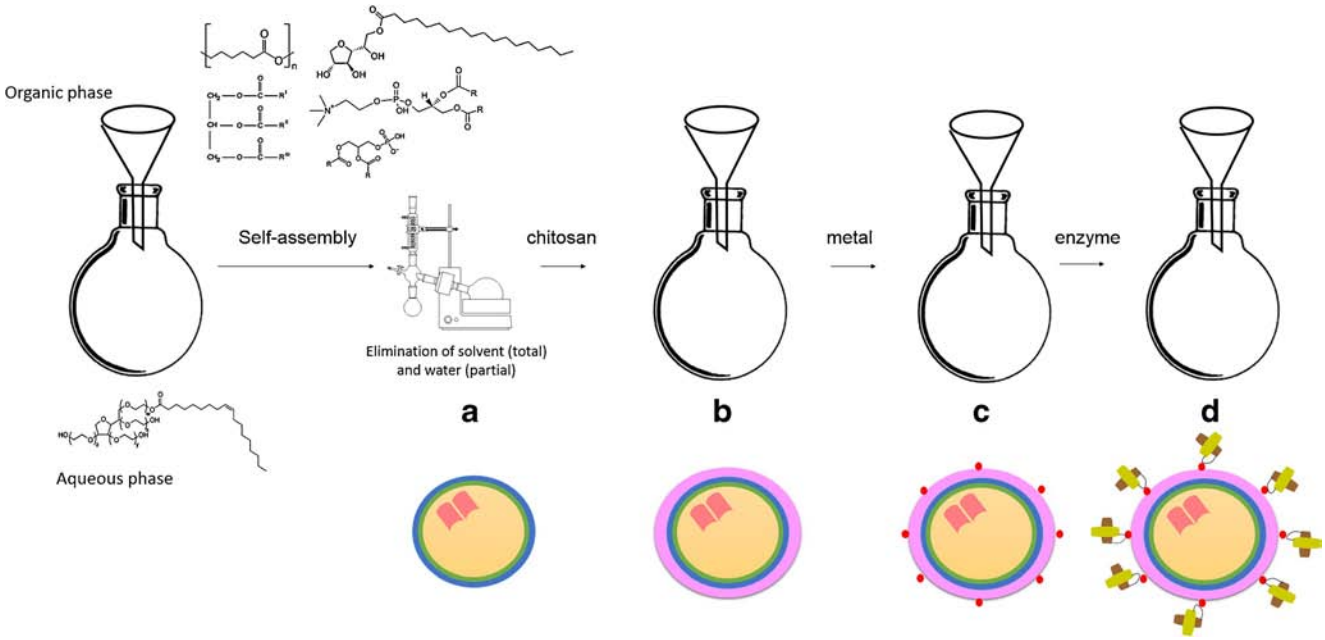


**Fig. 1** Schematic of one-pot synthesis and models of the supramolecular structure of **a**) lipid-core nanocapsules, **b**) chitosan-coated lipid-core nanocapsules, **c**) metal-chitosan multiple-wall lipid-core nanocapsules and **d**) laronidase-functionalized multiple wall lipid-core nanocapsules.

the samples directly into the wet unit. No filtration or centrifugation was performed to avoid sample selection. The granulometric profiles were determined by the corresponding volume and by the number of particles. The volume-weighted diameter average (D[4,3]) for each sample was determined by the Mastersizer 2000 software system, and the width of the particle size distribution (Span) was calculated using Eq. 1.

$$Span = \frac{d(0.9) - d(0.1)}{d0.5} \quad (1)$$

where d(0.1), d(0.5) and d(0.9) are the particle diameters at 10%, 50% and 90% of the undersized particle distribution curves as determined by the software system. The median diameter based on the particle number distribution was also determined [d(0.5)n].

The z-average diameter and polydispersity index (PDI) for each sample were determined by photon correlation spectroscopy (PCS) and the zeta potential was measured by electrophoretic mobility. Both procedures were performed with a Zetasizer Nano ZS (Malvern Instruments UK) at 20°C after diluting the samples with ultrapure water or 10 mmol $L^{-1}$ NaCl aqueous solution (no filtration or centrifugation was conducted after sample dilution). The pH of the formulations was determined by potentiometry (B474; Micronal, Brazil).

The physical stability of the formulations was performed by multiple light scattering using TurbiscanLab® equipment (Formulaction, France) (25). This equipment has an infrared source beam (λ=880 nm) and two detectors that simultaneously detect the transmitted light at 0° and the backscattered light at 135°. Transmission (T) and backscattering (BS) are acquired each 4 μm as a function of time from the bottom to the top of the cuvette containing the sample. The glass cells were filled with 10 mL of each sample without any treatment (dilution, centrifugation or filtration) and analyzed at 25°C within 1 and 24 h. A polystyrene latex suspension was used as an absolute backscattering standard (100% BS) and silicon oil was used as an absolute transmission standard (100% T). The relative backscattering profiles (ΔBS) of the samples were obtained using the provided software when the absolute transmission was lower than 0.2% with the first absolute BS scan as a reference.

## Enzyme Kinetic Properties

The kinetic properties of laronidase in solution and of laronidase-functionalized multiple-wall lipid-core nanocapsules (L-MLNC) were determined by a 4-methylumbelliferyl-α-L-iduronide fluorescent substrate in a microplate kinetic assay at 37°C for 40 min. Fluorescence measurements (λex=365 nm, λem=450 nm) were obtained at 20 s intervals. The substrate concentrations ranged from 0.23 mg $mL^{-1}$ to 0.014 mg $mL^{-1}$ and the assay was performed in a Spectramax M3 (Molecular Devices, USA). The final enzyme concentration used in the assay was 1.89 μg $mL^{-1}$. All tests were performed in triplicate in two independent experiments.

## *In Vitro* Cytotoxicity Analysis

The cytotoxicity of laronidase-functionalized multiple-wall lipid-core nanocapsules (L-MLNC) was evaluated with a

MTT (3-(4,5-dimethylthiazol-2-yl)-2,5-diphenyl tetrazolium bromide) (USB Corporation, USA) assay according to Mosmann *et al.* (26). The MPS I patient's fibroblasts were cultivated in Dulbecco's modified Eagle medium (DMEM, LGC, Brazil) supplemented with 10% fetal bovine serum (FBS, Gibco, USA) and 1% penicillin/streptomycin (standard culture conditions). When confluent, the cells were trypsinized and 5000 cells were plated in a 96-well plate (TPP, Switzerland) for 24 h before the assay ($n=3$). Laronidase concentrations ranging from 1.16 μg $mL^{-1}$ to 0.0058 μg $mL^{-1}$ either in solution or in L-MLNC plus an equivalent volume of LNC-$CS_{0.05}$ were incubated with fibroblasts for 24 h. After this period, each medium was removed and MTT solution (0.5 mg $mL^{-1}$) was added. After 4 h of incubation, 100 μL of dimethyl sulfoxide was added to dissolve the blue formazan crystals and the optical density was measured at 570 nm in a microplate reader (Anthos, Germany). Untreated fibroblasts were considered to have 100% cellular viability, and 0% cellular viability was obtained after incubating with Triton X-100 (10%, *w/v*). All tests were performed in 3 biological replicates.

### *In Vitro* Cell Uptake Analysis

The MPS I patient's fibroblasts were plated ($2 \times 10^5$ cells, n=5) and maintained under standard culture conditions for 24 h. After that, 0.0038 μg $mL^{-1}$ of laronidase either in solution or in L-MLNC was separately added to the medium. After 4 h incubation, the cells were washed with PBS three times to avoid that enzyme linked to the cell surface was measured. The cells were trypsinized, centrifuged and the pellet was resuspended in mili-q water. To ensure cells disruption, they were sonicated. The enzyme activity inside the cells was then measured by fluorescence assay (27) after incubation with 4-methylumbelliferyl-α-L-iduronide substrate (10 uL of a 2 mM solution) in 10 uL sodium formate buffer (pH 2.8) for 1 h (27). The reaction was stopped with glycine-NaOH buffer (pH 10.3) and measured in Spectramax M3 (λex=365 nm, λem=450 nm). Two standards with known IDUA concentration (positive controls) and a reaction without sample (negative control) were used for calculations. The proteins were measured by the Lowry method (28) and the units for enzyme activity were nmol/h/mg protein. To analyze the enzyme uptake mechanisms, the cells were also incubated in the presence of 5 mmol $L^{-1}$ mannose-6-phosphate (Sigma-Aldrich, USA), 3 μg $mL^{-1}$ filipin (Sigma-Aldrich, USA) and 50 μmol $L^{-1}$ chlorpromazine (Sigma-Aldrich, USA) or at 4°C for 1 h.

### Clearance and Biodistribution

Four-month-old *Idua*$^{-/-}$ mice received laronidase (0.085 μg $g^{-1}$) either in solution or in L-MLNC via their tail veins in a 200 μL volume. To determine the enzyme's clearance from blood circulation, 30 μL blood samples were collected under isoflurane anesthesia at 5, 10, 15, 30, 60, 90, 120, 180 and 240 min after infusion. After blood centrifugation at 3000 rpm for 10 min, the serum was collected, and 10 uL were incubated with 10 uL of fluorescent substrate 4-methylumbelliferyl-α-L-iduronide (2 mM.) for 1 h. The reaction was stopped with glycine-NaOH buffer (pH 10.3) and measured in Spectramax M3 (λex=365 nm, λem=450 nm). Two standards with known IDUA concentration (positive controls) and a reaction without sample (negative control) were used for calculations. The units were nmol/h/mL of serum.

The area under the curve was measured by SigmaPlot version 11.0. The enzyme clearance profile (between 5 and 240 min, n=3) was modeled according to the monoexponential equation (Eq. 2) using MicroMath® Scientist® for Windows™ software (Version 3.0, Jandel Scientific, USA). The correlation coefficient was higher than 0.97 for all analyzed profiles. The half-life time ($t_{1/2}$) of enzyme decay was calculated (n=3) according to Eq. 3 using the decay constant calculated by Eq. 2.

$$C = C_0 \times e^{-kt} \tag{2}$$

where k is the decay constant, $C_0$ is the initial enzyme concentration and C is the enzyme concentration at time t.

$$t_{1/2} = 0.693/k \tag{3}$$

where k is the rate of enzyme decay ($m^{-1}$).

The animals were sacrificed at 4 h ($n=3$/group) or 24 h ($n=3$/group) after injection to determine the biodistribution. The animals were anesthetized with isofluorane and perfused with 20 mL of phosphate saline buffer. After this procedure, the liver, kidney, spleen, lungs, heart, and brain were collected and maintained at −80°C until enzyme activity analysis, which was performed by incubating macerated and sonicated tissue with the substrate 4-methylumbelliferyl-α-L-iduronide as described above. The proteins were measured by the Lowry method (28) and the units for enzyme activity were nmol/h/mg protein.

### Statistical Analysis

A statistical analysis was performed by Predictive Analytics software (PASW, version 18.0). The tests are specified on the results description and/or on table/figure legends. Significant differences among groups were defined as $p<0.05$.

## RESULTS

### Lipid Core Nanocapsules as Building Blocks to Multiple-Wall Nanocapsules

The lipid-core nanocapsules (LNC) appeared as cloudy white homogeneous colloidal suspensions. The cloudy white appearance was maintained after chitosan coating. The pH of the colloidal suspensions ranged from 3.4±0.16 (LNC-$CS_{0.075}$) to 3.7±0.05 (LNC-$CS_{0.03}$), which was significantly lower than the pH 6.4±0.04 observed for LNC ($p<0.05$). After coating with chitosan, the pH value decreased because of the acetic acid solution that was used to dissolve the polysaccharide.

The LNC had a unimodal and narrow size distribution with a D[4,3] of 130 nm and a SPAN value lower than 1.0 (Table I). Following the chitosan coating, unimodal and narrow size distributions were only observed for LNC-$CS_{0.05}$ and LNC-$CS_{0.075}$, while LNC-$CS_{0.03}$ presented a multimodal profile (Suppl. figure 1). As a consequence, the D[4,3] for LNC-$CS_{0.03}$ was 641±164 nm, whereas LNC-$CS_{0.05}$ and LNC-$CS_{0.075}$ showed lower values close to 140 nm (Table I). The polydispersity was calculated as a SPAN with values of 2.7±0.8 for LNC-$CS_{0.03}$, but lower than 1.2 for LNC-$CS_{0.05}$ and LNC-$CS_{0.075}$ (Table I). The zeta potential value for LNC was negative, and the values for LNC-$CS_{0.05}$ and LNC-$CS_{0.075}$ were positive, indicating efficient coatings with chitosan (Table I). However, LNC-$CS_{0.03}$ had a zeta potential of −1.7±7 mV. This result and the one obtained by laser diffraction indicated there was an insufficient amount of chitosan to cover the colloidal surface in LNC-$CS_{0.03}$.

The LNC-$CS_{0.05}$ and LNC-$CS_{0.075}$ formulations were selected for further physico-chemical characterization. The d(0.5)n values were lower than 100 nm for both formulations (Table I). The values were similar ($p>0.05$) to that calculated for LNC (Table I).

The formulations were analyzed by PSC to better characterize the nanoscopic population. The z-average diameters and polydispersity index (PDI) were calculated by the cumulant method. The intensity profiles were unimodal and the z-average diameters were slightly higher after chitosan coating (Table I). The polydispersity indexes were lower than 0.2 (Table I) indicating homogeneous and narrow particle size distributions.

### Laronidase-Functionalized Multiple-Wall Lipid-Core Nanocapsules

The LNC formulations coated with chitosan exhibited narrow size distributions, and those with a slight increase in the D[4,3] values and positive zeta potential were chosen to be functionalized with laronidase. Thus, four different formulations were obtained by using different laronidase concentrations (Table II). All formulations of multiple-wall nanocapsules had an opalescent appearance, a Tyndall effect and no precipitation.

After the interfacial enzyme reactions, the formulations had a pH value close to that of the commercial enzyme, with values ranging from 4.1±0.08 for $L_1$-$MLNC_1$ to 4.2±0.07 for $L_2$-$MLNC_2$. Fig. 2 shows the size distribution profiles as based either on the volume of the equivalent sphere or on the number of particles. The d(0.5)n values were lower than 100 nm for all formulations. For the $L_1$-$MLNC_1$ and $L_2$-$MLNC_2$ formulations, the unimodal particle size distributions remained in the nanometric range, with D[4.3] values of 134 ±3 nm and 137±4 nm, respectively; whereas small populations of micrometric particles were observed for $L_2$-$MLNC_1$ and $L_1$-$MLNC_2$ besides the nanoscopic populations when the profiles were analyzed on the basis of volume. Therefore, only $L_1$-$MLNC_1$ and $L_2$-$MLNC_2$ were considered suitable for further analysis because these formulations had unimodal nanoscopic particle distributions, while $L_2$-$MLNC_1$ and $L_1$-$MLNC_2$ had multimodal particle distributions. The PCS profiles of those formulations showed narrow populations with z-average diameters of 71±1 nm and 79±1 nm, respectively, and polydispersity indexes lower than 0.2 (Table III).

The laronidase in aqueous solution and the $L_1$-$MLNC_1$ and $L_2$-$MLNC_2$ formulations were analyzed by PCS. The distribution profiles were determined as a function of the intensity, volume and number. A comparison between the free and nanostructured laronidase profiles verified that the free enzyme solution had multimodal size distributions (Fig. 3a), which may represent enzyme aggregates, since laronidase molecular

**Table I** The Volume Weighted Diameter Average (D[4,3]), Polydispersity (SPAN), and Median Diameter based on the Particle Number Distribution [d(0.5)n], Z-average Diameter (z-ave), Polydispersity Index (PDI) and Zeta Potential. Data are Presented as Means ± Standard Deviation, with $n=3$ for each Formulation. ANOVA with Tukey's post hoc Test

| Formulation | D[4,3] (nm) | SPAN | d(0.5)n (nm) | (z-ave) (nm) | PDI | Zeta potential (mV) |
|---|---|---|---|---|---|---|
| LNC | 130±2 | 0.9±0 | 89±3 | 67±5# | 0.12±0.02 | −11.1±4* |
| LNC-$CS_{0.05}$ | 140±8 | 1.2±0.2 | 71±6 | 73±1 | 0.15±0.01 | +10.8±5 |
| LNC-$CS_{0.075}$ | 133±1 | 1.0±0.1 | 84±3 | 76±2 | 0.17±0.01 | +16.2±2 |

*$p<0.05$ when compared with other formulations. #$p<0.05$ when compared with LNC-CS0.075.

**Table II** Multiple-Wall Nanocapsule Composition

| Formulation | Chitosan concentration | Laronidase concentration (μg/mL) |
|---|---|---|
| $L_1$-MLNC$_1$ | 0.050% | 11 |
| $L_2$-MLNC$_1$ | 0.050% | 96 |
| $L_1$-MLNC$_2$ | 0.075% | 11 |
| $L_2$-MLNC$_2$ | 0.075% | 96 |

weight is 83 kDa. Laronidase-functionalized multiple-wall lipid-core nanocapsules present unimodal distributions (Fig. 3b), which ranged from 25 nm to 229 nm by intensity for $L_1$-MLNC$_1$ (peak width of 204 nm), and from 25 nm to 308 nm for $L_2$-MLNC$_2$ (peak width of 283 nm) (Fig. 3). These results suggested that the enzyme was bound to the nanocapsule surface that presented similar homogeneous size distributions to those of the chitosan-coated lipid-core nanocapsules. The z-average diameter did not vary after the interfacial reaction of the enzyme with the metal-chitosan multiple-wall lipid-core nanocapsules (Student's t-test, $p>0.05$).

Multiple light scattering analysis was used to assess the formulation stability. Because the signal transmission was zero as a function of time, the relative backscattering profiles were

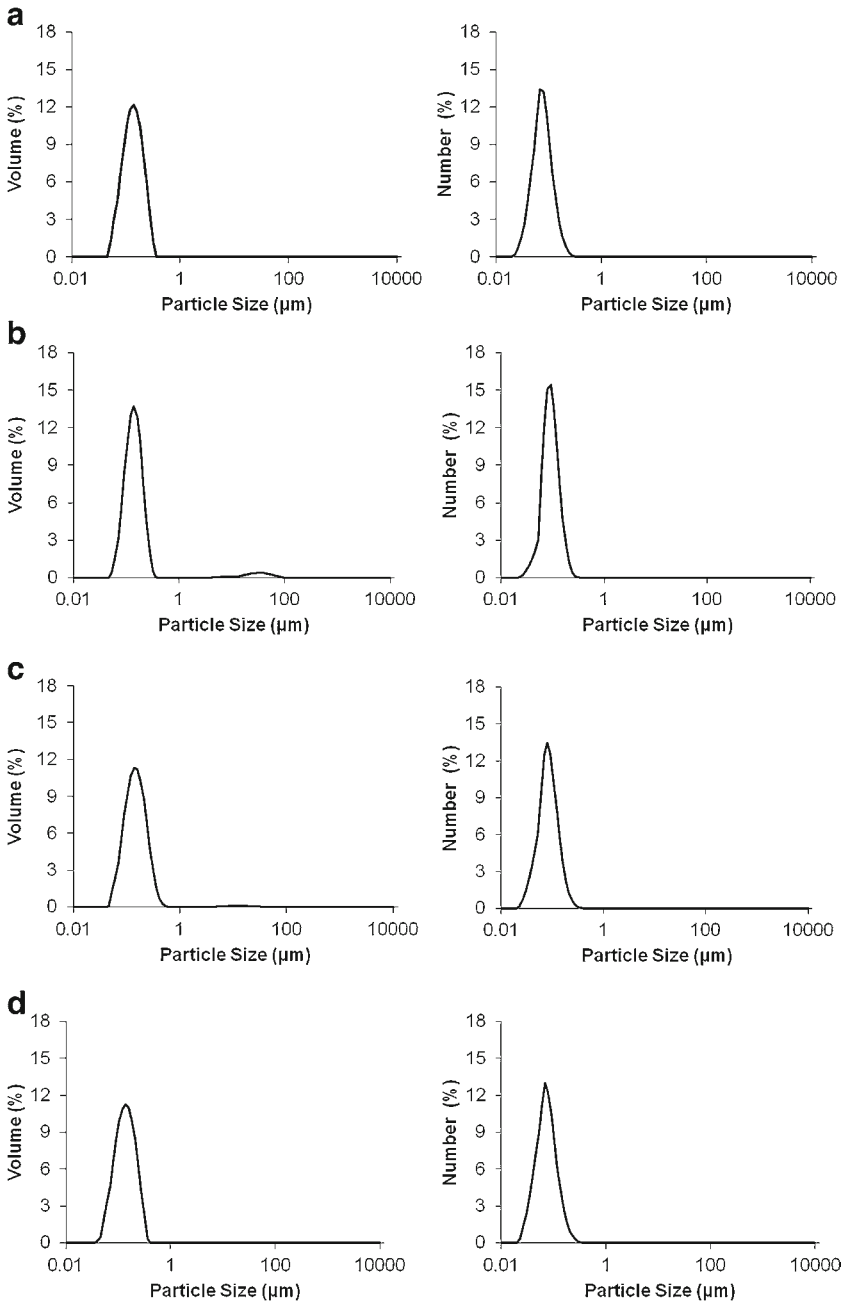


**Fig. 2** The particle size distribution as obtained by laser diffraction. (**a**). $L_1$-MLNC$_1$; (**b**). $L_2$-MLNC$_1$; (**c**). $L_1$-MLNC$_2$ and (**d**). $L_2$-MLNC$_2$ ($n=3$ for each formulation). $L_1$-MLNC$_1$ and $L_2$-MLNC$_2$ had all particles diameters smaller than 1 μm, while $L_2$-MLNC$_1$ and $L_1$-MLNC$_2$ showed two populations of particles, one smaller than 1 μm and the other close to 10 μm when analyzed by volume.

**Table III** Mean Size (D[4,3]), SPAN, Mean Diameter and PDI of Multiple Wall Lipid Core Nanocapsules ($n = 3$ for each Formulation)

| Formulation | D[4,3] (nm) | SPAN | d(0.5)n (nm) | (z-ave) | PDI |
|---|---|---|---|---|---|
| $L_1$-MLNC$_1$ | 134 ± 3 | 1.2 ± 0 | 70 ± 5 | 71 ± 1 | 0.14 ± 0.01 |
| $L_2$-MLNC$_1$ | 352 ± 169 | 1.3 ± 0.1 | 76 ± 14 | – | – |
| $L_1$-MLNC$_2$ | 1530 ± 1383 | 1.1 ± 0.2 | 83 ± 11 | – | – |
| $L_2$-MLNC$_2$ | 137 ± 4 | 1.2 ± 0.1 | 67 ± 4 | 79 ± 1 | 0.16 ± 0.01 |

analyzed. Both formulations showed a slight increase in the ΔBS signal at the base of the optical cells followed by a slight reduction at the top. No significant changes were observed in the BS signal at the center of the optical cells after 1 h or 24 h (Suppl. fig. 2).

## Enzyme Kinetic Properties

The enzyme activities of $L_1$-MLNC$_1$ and $L_2$-MLNC$_2$ formulations were verified to guarantee that the active site was not lost after complexation. The $L_2$-MLNC$_2$ formulation showed reduced enzyme activity when compared with either $L_1$-MLNC$_1$ or laronidase (data not shown). Thus, the kinetic properties were determined only for the $L_1$-MLNC$_1$ formulation and compared with the laronidase solution. Table IV shows the results for the Km, Vmax, Kcat, Ecat and the amount of the final product. There was no significant difference between the Km of laronidase and that of $L_1$-MLNC$_1$. Surprisingly, the other parameters were significantly higher for $L_1$-MLNC$_1$ than for the laronidase solution. The free laronidase in solution and laronidase-functionalized multiple-wall lipid-core nanocapsules had different properties.

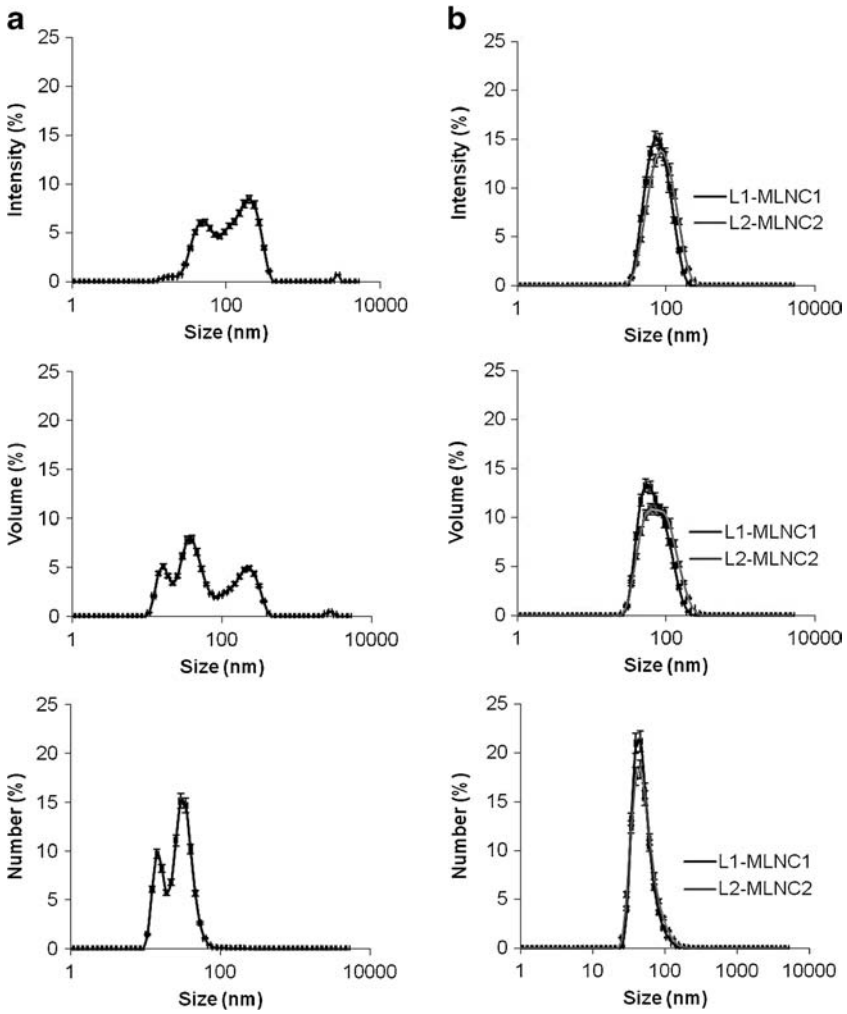


**Fig. 3** Size distribution profiles by photon correlation spectroscopy as functions of the intensity, volume and number. (**a**). Laronidase and (**b**). $L_1$-MLNC$_1$ and $L_2$-MLNC$_2$ ($n = 3$ for each formulation).

**Table IV** Catalytic Properties of Laronidase and Laronidase-Functionalized Multiple-Wall Lipid-Core Nanocapsules ($L_1$-$MLNC_1$)

| | Laronidase | L1-MLNC1 |
|---|---|---|
| Km ($\mu$M) | 127.93 ± 38.00 | 105.18 ± 17.89 |
| Vmax ($\mu$M.s-1) | 1.01 ± 0.22 | 1.45 ± 0.16* |
| Kcat (s-1) | 36.48 ± 7.87 | 53.55 ± 6.07* |
| Ecat (s-1 $\mu$M-1) | 0.29 ± 0.07 | 0.51 ± 0.06* |
| Final product ($\mu$M) | 575.23 ± 70.80 | 753.38 ± 13.24* |

*$p < 0.05$, Student's t-Test

### *In Vitro* Cytotoxicity Analysis

The cytotoxicity of laronidase-functionalized multiple-wall lipid-core nanocapsules was evaluated by MTT assay using MPS I patient's fibroblasts, which were cultivated in concentrations ranging from 1.16 µg/mL to 0.0058 µg/mL of laronidase, LNC-$CS_{0.05}$ or $L_1$-$MLNC_1$ (Suppl. fig. 3). Laronidase caused no cytotoxicity at any of the tested concentrations. Both $L_1$-$MLNC_1$ and LNC-$CS_{0.05}$ caused approximately 30% cell death at higher concentrations, but they reached 90-100% cell viability at concentrations lower than 0.232 µg/mL and 0.0232 µg/mL, respectively.

### *In Vitro* Cell Uptake Analysis

The capacity of laronidase or $L_1$-$MLNC_1$ uptake by cells was analyzed*in vitro* by adding the enzymes to the medium with the MPS I patient's fibroblasts. Both forms of laronidase could be internalized, thereby restoring normal enzyme activity levels inside the MPS I patient's fibroblasts (Suppl. fig. 4).

The MPS I patient's fibroblasts were submitted to different protocols to verify the cell uptake mechanisms through which $L_1$-$MLNC_1$ was internalized. Alpha-L-iduronidase is taken up by mannose-6-phosphate receptors (clathrin-mediated endocytosis), which was confirmed by the reduced intracellular activity of laronidase after incubating with mannose-6-phosphate (Fig. 4). However, no decrease in enzyme activity was observed for $L_1$-$MLNC_1$. Active transport inhibition was performed to verify the possibility of $L_1$-$MLNC_1$ membrane diffusion. Although incubation at 4°C only reduces cellular metabolism, the decrease in the enzyme uptake was similar for laronidase and $L_1$-$MLNC_1$ was similar, leading to conclusion that $L_1$-$MLNC_1$ does not enter the cell by passive transport. (Fig. 4). To assess the possibility that $L_1$-$MLNC_1$ was being internalized by caveolin or clathrin-mediated endocytosis, an incubation with filipin or chlorpromazine (specific caveolin and clathrin-mediated endocytosis inhibitors, respectively) was performed. As expected, laronidase uptake diminished only after chlorpromazine treatment, but no difference was observed in $L_1$-$MLNC_1$ uptake after both treatments.

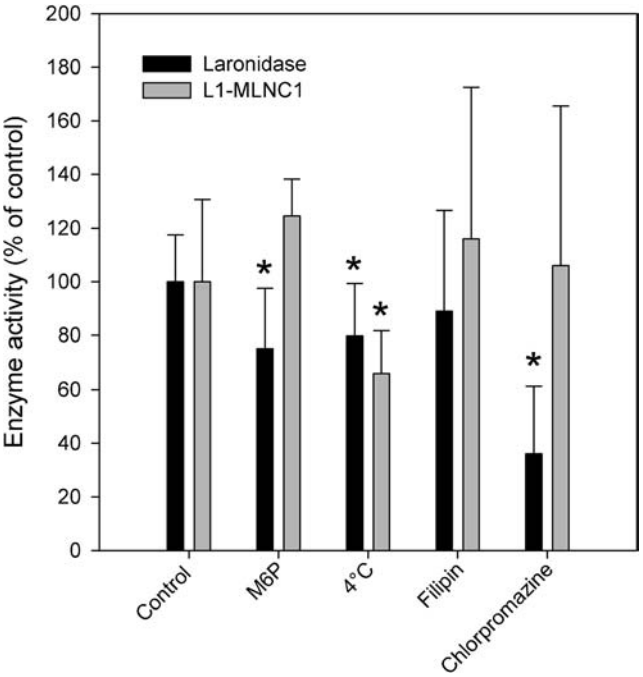


**Fig. 4** Uptake mechanisms of $L_1$-$MLNC_1$. MPS I fibroblasts were incubated with laronidase or $L_1$-$MLNC_1$ at 37°C (control groups) and with 5 mM mannose-6-phosphate, 3 $\mu$g/mL filipin, 50 $\mu$M chlorpromazine at 4°C. Intracellular enzyme activity was measured by fluorescent methods, *$p < 0.05$ when compared with the control group by Student's t-Test.

### Clearance and Biodistribution

To assess clearance from circulation and biodistribution within tissues, 0.085 µg/g body weight of laronidase or $L_1$-$MLNC_1$, was injected i.v. into 4-month-old *Idua*$^{-/-}$ mice ($n = 3$/group/time). The serum enzyme activity from the animals that received $L_1$-$MLNC_1$ was higher than those who received laronidase, with an area under the curve that was over three-fold higher ($p < 0.01$), but there was no difference in the half-life time (Fig. 5, Table V). The intravenously administered enzyme was detectable in the circulation 4 h after injection, and the enzyme activity was almost nil after 24 h for both groups (data not shown).

The enzyme activity was measured in five peripheral organs and in the central nervous system (CNS). Four hours after injection, the animals who received $L_1$-$MLNC_1$ presented higher enzyme activity in the liver, spleen and heart ($p < 0.05$) (Fig. 6a). Interestingly, the enzyme activity was higher after 24 h, not only in the liver but also in the kidney (Fig. 6b). There was no significant difference between the animals that received laronidase or $L_1$-$MLNC_1$ at 24 h in the spleen, heart and lungs. There was no difference in the enzyme activity in the CNS at either 4 h or 24 h after infusion.

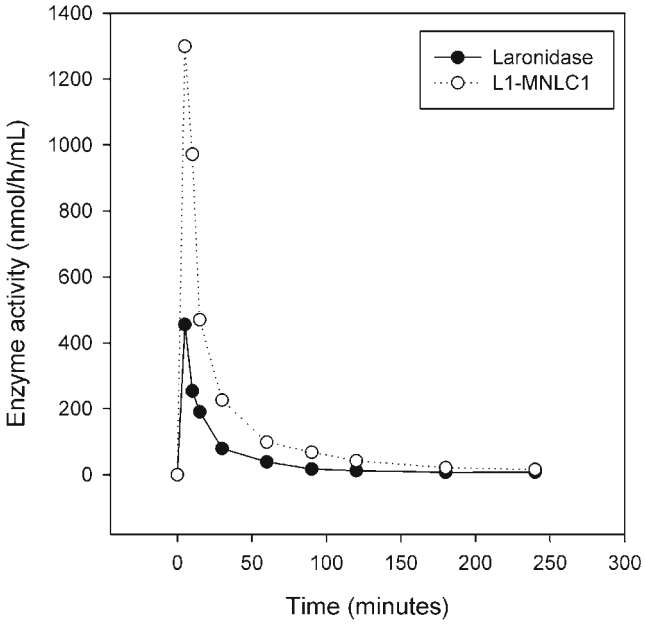


**Fig. 5** Serum clearance of laronidase and $L_1$-$MLNC_1$ over 4 h after infusion in MPS I mice (0.085 $\mu$g/g of body weight, $n = 3$/group/time).

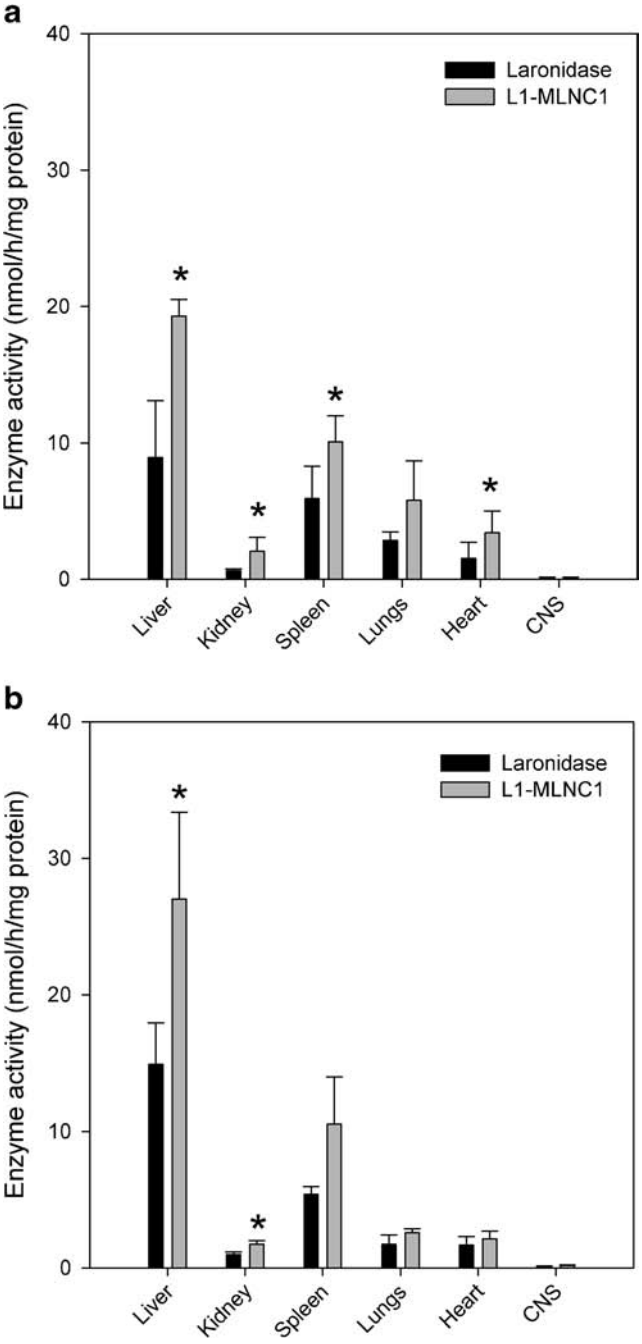


**Fig. 6** Biodistribution of laronidase and $L_1$-$MLNC_1$ in MPS I mice. (**a**). 4 h after infusion. (**b**). 24 h after infusion. (0.085 $\mu$g/g of body weight, $n = 3$/group/time). *$p < 0.05$ when compared with laronidase at the same time point, Student's t-test.

## DISCUSSION

In this study, we proposed a new strategy for binding a ligand to the surface of a biodegradable nanoparticle. The multiple-wall lipid core nanocapsules were developed to bind an enzyme (laronidase) and improve its pharmacokinetic and biodistribution parameters. In the first stage of nanoparticle development, LNCs were coated with three different concentrations of chitosan. The inversion of the zeta potential and size distribution at the nanoscale indicated that proper coating with chitosan occurred for LNC-$CS_{0.05}$ and LNC-$CS_{0.075}$. A particle sizing analysis (by number) showed mean diameters lower than 100 nm, indicating that the colloidal suspensions were in accordance with the European Union concept of a nanostructure material (29). In addition, the PCS analysis showed that LNC-$CS_{0.075}$ had a higher diameter when compared with $LNC_{0.05}$, indicating a thicker layer of chitosan in this formulation. Similar results were also observed by Siqueira *et al.* (30), who showed that coating polymeric nanocapsules with a cationic layer of chitosan caused both the inversion of the zeta potential and the enhancement of the mean diameter.

The LNC-$CS_{0.05}$ and LNC-$CS_{0.075}$ suspensions were selected to continue the study because they provided the best cationic coating profiles. An Iron II solution was added to each suspension followed by the interfacial reaction of laronidase as tested in two different concentrations. Laser diffraction analysis and photon correlation spectroscopy

**Table V** Clearance Characteristics of Laronidase and $L_1$-$MLNC_1$. The Area Under the Curve was Over Three-fold Higher ($p < 0.01$, Student t Test) for $L_1$-$MLNC_1$, and there was no Difference in the Half-Life Time

| | Laronidase | $L_1$-$MLNC_1$ |
|---|---|---|
| Area under the curve | 2883.87 ± 399.18 | 9459.83 ± 1290.77* |
| Half-life time (min) | 11.46 ± 5.14 | 11.72 ± 3.27 |

*$p < 0.05$, Student's t-test

confirmed the formation of stable nanosized particles. Maintaining the size in the nanometer range is important for compatibility with the administration route. Moreover, the monomodal profiles observed after enzyme addition showed that the high affinity between iron and laronidase allowed for the enzyme's complete chemisorption at the nanocapsule surface, promoting the formation of a hybrid structure. The supramolecular structure model consists of a lipid-core nanocapsule with polyester as the first wall (9) and it is coated with a negative layer from a phosphatidic acid (which is a contaminant in lecithin) (30) that is covered by a chitosan wall electrostatic interaction, which in turn coordinates iron with the specific enzyme chemisorption site.

After the interfacial reaction of the enzyme, the pH of the formulation remained close to that of the commercial enzyme (aqueous solution). Maintaining the pH is an important aspect in developing carriers for biomolecule binding, especially enzymes, to retain functional conformation and activity (31). Because laronidase is a lysosomal enzyme, the acid pH observed for the nanocapsule formulation is important for maintaining optimal enzyme activity (27).

A stability analysis by multiple light scattering showed that both $L_1$-$MLNC_1$ and $L_2$-$MLNC_2$ were kinetically stable formulations. The slight sedimentation observed is a consequence of the larger particles in suspension. The destabilization phenomena are detected, for example for particle sedimentation, when there is a positive relative BS signal on the base and a negative relative BS signal on the top (32). Brownian movement guaranteed the physical stability of the colloidal formulations. Furthermore, the results indicated a high chemical stability at the nanocapsule surface because no variation at the center of the optical cells was observed (no flocculation occurred). No changes in the BS signal at the center of the optical cells are desirable because those variations are related to the irreversible destabilizations that involve particle size changes, such as coalescence, flocculation and aggregation (25). The sedimentation value lower than 3% and the lack of variation at the center of the cells showed that no flocculation occurred for either formulation. These results indicated that the passivation at the nanocapsule surface after reacting with laronidase was satisfactory, yielding (relatively) kinetically stable colloidal suspensions.

The enzyme activity of both $L_1$-$MLNC_1$ and $L_2$-$MLNC_2$ was analyzed and compared with laronidase. The $L_2$-$MLNC_2$ formulation showed a reduced activity in comparison with $L_1$-$MLNC_1$ or laronidase. These results suggested that the higher enzyme concentration at the nanocapsule surface for $L_2$-$MLNC_2$ generated a steric hindrance, preventing the arrival of the substrate to the active site of the enzyme. Thus, only the catalytic properties of $L_1$-$MLNC_1$ and laronidase were studied. There was no significant difference between the Km of $L_1$-$MLNC_1$ and laronidase, and the Kcat (Vmax/enzyme concentration) and catalytic efficiency (Ecat - Kcat/Km) were higher for $L_1$-$MLNC_1$. These superior properties ensured that a greater amount of product was obtained from the same substrate concentration, indicating that laronidase-functionalized multiple-wall lipid-core nanocapsules are an innovative formulation with enzyme catalytic activity that is more efficient. One possible explanation for the superior catalytic properties of $L_1$-$MLNC_1$ may rely in the fact that laronidase apparently form aggregates, as suggested by the PCS data, which shows that average size of laronidase is more than 50 nm. This hypothesis is supported by the results which show that nanocapsules with higher laronidase concentrations had lower enzyme activity. Therefore, nanostructuration process may enable the active sites from a larger number of enzyme units to be exposed, leading to a higher catalytic efficiency.

Nano-sized particles have been used as enzyme supporting materials to improve enzyme capabilities because of their unique size and physical properties (33). However, a decrease in the enzyme activity is expected if essential amino acid residues located close to the active site are involved in the conjugation process (34). Hong *et al.* (35) showed that enzyme activity is influenced by the nature of the nanocarrier surface. These investigators observed that chymotrypsin could be inhibited after forming a nanostructure either by denaturation or by retaining its structure. We used interactions with a chitosan-metal complex to obtain a nanostructured enzyme. This approach is appropriate because of the non-covalent conjugation, but it is coordination bound, which promotes better specificity because the transition metals are able to form complexes with the side chains of amino acid residues containing imidazole groups (3). In previous work, Abad *et al.* (36) developed gold nanoparticles coated with $Co^{2+}$ that were efficiently complexed to two enzymes, exhibiting histidine residues on its N-terminal. Enzyme binding was prevented by eliminating these residues. We observed an improvement in the laronidase catalytic properties that can be attributed to its binding to the nanocapsules. Despite the presence of histidine residues within the active site of IDUA (37), the interaction with iron most likely occurred on the inert regions of the enzyme.

After the enzyme properties characterization, *in vitro* studies were performed to describe the cytotoxicity and cell uptake mechanism. A cytotoxicity analysis was performed on the MPS I patient's fibroblasts using different concentrations of laronidase, $L_1$-$MLNC_1$ or LNC-$CH_{0.05}$. Laronidase did not cause cell death, and both $L_1$-$MLNC_1$ and LNC-$CH_{0.05}$ caused approximately 30% cell death at higher concentrations, but achieved 100% cell viability with concentrations latter used for *in vivo* tests. Cationic polymer nanoparticles can be toxic at high concentrations (38). However, the hemocompatibility of chitosan-coated nanocapsules previously exhibited a low toxicity because of the low polysaccharide concentration used in the formulation (18). Moreover, the

usual enzyme dose provided to patients is 1.2 μg/g body weight (39) every two weeks. We tested 1.16 μg/mL medium in 5000 cells and observed 30% cell death. This was a promising result for the implementation of this dose for *in vivo* studies.

Because $L_1$-$MLNC_1$ had no significant cytotoxicity, *in vitro* experiments were performed to compare the laronidase and $L_1$-$MLNC_1$ uptake. There was no difference in the enzyme activity on the MPS I patient's fibroblasts after treating with both enzymes (Suppl. figure 4). This finding indicates that $L_1$-$MLNC_1$ is active in a biological system and can be internalized by the patient's cells. However, unlike laronidase, $L_1$-$MLNC_1$ is internalized by a pathway other than the mannose-6-phosphate receptor. Although we were not able to characterize this pathway completely, we ruled out passive diffusion or caveolin-mediated endocytosis.

Finally, *in vivo* pharmacokinetics studies were performed to evaluate if the improved catalytic properties of $L_1$-$MLNC_1$ influenced the clearance and biodistribution profiles. *Idua*$^{-/-}$ mice received 0.085 μg /g body weight of laronidase or $L_1$-$MLNC_1$. This concentration, although lower than the therapeutic dose (1.2 μg/g body weight), corresponds to a maximum volume of 200 μL for an animal of approximately 25 g because the optimal enzyme concentration in the nanostructured formulations was 11 μg/mL. The enzyme activity in animals that received $L_1$-$MLNC_1$ was higher at all analyzed times, indicating that $L_1$-$MLNC_1$ was able to change the enzyme pharmacokinetic profile, thereby increasing the circulation time of the active enzyme. In addition, $L_1$-$MLNC_1$ was also responsible for a higher enzyme activity in the peripheral organs (Figure 6). However, the modified enzyme was not able to cross the blood brain barrier, most likely because its mechanism of internalization is mediated by active transport based on receptors that are not expressed on the vascular endothelia of the central nervous system.

Enzyme nanostructuration is a relatively new approach, but the field has an increasing number of studies. In 2008, Garnacho *et al.* (40) showed that the use of polymer carriers that were targeted with anti-ICAM-1 for acid sphingomyelinase (EC 3.1.4.12) had quick, uniform and efficient binding to the endothelium after intravenous injection in mice. The investigators observed a rapid clearance and increased accumulation of nanostructures when compared with free enzymes in the kidney, heart, liver, spleen and lungs, showing a possible improvement in ERT for Niemann-Pick type B (OMIM # 607616) (40). Another pre-clinical study using enzyme nanostructures was performed with α-galactosidase (E.C.3.2.1.22) in a murine model of Fabry disease. Mice treated with a nanocarrier and also targeted with anti-ICAM-1 had greater α-galactosidase activity in the brain, kidney, heart, liver, lungs and spleen, in addition to vascular endothelial cells. Endocytosis and the lysosomal transport of the nanostructures were also shown, in addition to the increased degradation of globotriaosylceramide, the substrate accumulated in Fabry disease (41). Both studies employed nanocarriers to bind to a specific molecule. In the present work, we developed a nanocarrier system based on laronidase interactions with metal to obtain a nanostructured lysosomal enzyme, which showed improved catalytic properties in addition to better clearance and biodistribution profiles.

Although the given formulation could not overcome one of the great limitations of ERT, that is, reaching the CNS, it can be beneficial for addressing two other negative aspects of ERT. One limitation is the need for high concentrations of enzyme that may be involved in the immunological response observed in many patients and that require the administration of antipyretics and/or antihistamines before enzyme infusion (24). Because nanostructures enable the achievement of a higher activity from smaller amounts of drugs, it is likely that it will reduce these effects and costs by decreasing the dose (3). Thus, a possible dose decrease can provide a weaker immune response and a cost reduction, which would make ERT available more quickly to patients. In this sense, the system developed in this study can help to address the high costs of ERT for MPS I patients.

## CONCLUSIONS

In this work, we synthesized laronidase surface-functionalized lipid-core nanocapsules to overcome some of the limitations of ERT for treating Mucopolysaccharidosis I. The advantages of this new strategy are as follows: an easy one-pot process, flexibility in the functionalization and no need for purification. The use of lipid-core nanocapsules as building blocks for producing functionalized multiple-wall nanocapsules represents a new platform for producing decorated soft nanoparticles with a narrow size distribution, excellent reproducibility and particle homogeneity. The innovative nanocapsules proved to be more effective than commercial laronidase because the enzyme catalytic properties were improved, and *in vivo* studies on biodistribution and clearance showed superior results for the innovative formulation. It is worth noting that the dose used in this study was lower than the one usually administered to the patients, and thus more investigations regarding dose adjustment and therapeutic efficacy are needed.

## ACKNOWLEDGMENTS AND DISCLOSURES

The authors are grateful for the financial support of the *Fundo de Incentivo à Pesquisa* (FIPE-HCPA), PRONEX and PRONEM FAPERGS/CNPq, INCT-if CNPq, Universal CNPq, FAPERGS and Rede Nanobiotec CAPES. The sponsors had no involvement in the study design, data collection,

analysis, interpretation, writing and decision to publish the data.

## REFERENCES


1. Tan ML, Choong PF, Dass CR. Recent developments in liposomes, microparticles and nanoparticles for protein and peptide drug delivery. Peptides. 2010;31(1):184–93.
2. Carino GP, Jacob JS, Mathiowitz E. Nanosphere based oral insulin delivery. J Control Release. 2000;65(1–2):261–9.
3. Torchilin VP. Drug targeting. Eur J Pharm Sci. 2000;11 Suppl 2: S81–91.
4. Caruthers SD, Wickline SA, Lanza GM. Nanotechnological applications in medicine. Curr Opin Biotechnol. 2007;18(1):26–30.
5. Kreuter J. Nanoparticulate systems for brain delivery of drugs. Adv Drug Deliv Ver. 2001;47(1):65–81.
6. Di Marco M, Shamsuddin S, Razak KA, *et al.* Overview of the main methods used to combine proteins with nanosystems: absorption, bioconjugation, and encapsulation. Int J Nanomedicine. 2010;5: 37–49.
7. Jonkheijn P, Weinrich D, Schröder H, Niemeyer CM, Waldmann H. Chemical strategies for generating protein biochips. Angew Chem Int Ed Engl. 2008;47(50):9618–47.
8. Rana S, Yeh YC, Rotello VM. Engineering the nanoparticle–protein interface: applications and possibilities. Curr Opin Chem Biol. 2010;14(6):828–34.
9. Jager E, Venturini CG, Poletto FS, *et al.* Sustained release from lipid-core nanocapsules by varying the core viscosity and the particle surface area. J Biomed Nanotechnol. 2009;5(1):130–40.
10. Venturini CG, Jäger E, Oliveira CP, *et al.* Formulation of lipid core nanocapsules. Colloids and Surf A: Physicochem Eng Aspects. 2011;375:200–8.
11. Jornada DS, Fiel LA, Bueno K, *et al.* Lipid-core nanocapsules: mechanism of self-assembly, control of size and loading capacity. Soft Matter. 2012;8:6646–55.
12. Fiel LA, Rebelo LM, Santiago TM, *et al.* Diverse deformation properties of polymeric nanocapsules and lipid-core nanocapsules. Soft Matter. 2011;7:7240–7.
13. Bernardi A, Frozza RL, Horn AP, *et al.* Protective effects of indomethacin-loaded nanocapsules against oxygen-glucose deprivation in organotypic hippocampal slice cultures: involvement of neuroinflammation. Neurochem Int. 2010;57(6):629–36.
14. Bernardi A, Zilberstein AC, Jager E, *et al.* Effects of indomethacin-loaded nanocapsules in experimental models of inflammation in rats. Br J Pharmacol. 2009;158(4):1104–11.
15. Bernardi A, Braganhol E, Jager E, *et al.* Indomethacin-loaded nanocapsules treatment reduces *in vivo* glioblastoma growth in a rat glioma model. Cancer Lett. 2009;281(1):53–63.
16. Ourique AF, Azoubel S, Ferreira CV, *et al.* Lipid-core nanocapsules as a nanomedicine for parenteral administration of tretinoin: development and *in vitro* antitumor activity on human myeloid leukaemia cells. J Biomed Nanotechnol. 2010;6(3):214–23.
17. Frozza RL, Bernardi A, Paese K, *et al.* Characterization of trans-resveratrol-loaded lipid-core nanocapsules and tissue distribution studies in rats. J Biomed Nanotechnol. 2010;6(6):3694–703.
18. Bender EA, Adorne MD, Colome LM, *et al.* Hemocompatibility of poly(epsilon-caprolactone) lipid-core nanocapsules stabilized with polysorbate 80-lecithin and uncoated or coated with chitosan. Int J Pharm. 2012;426(1–2):271–9.
19. Bender EA, Cavalcante MF, Adorne MD, *et al.* New strategy to surface functionalization of polymeric nanoparticles: one-pot synthesis of scFv anti-LDL(-)-functionalized nanocapsules. Res: Pharm; 2014. doi:10.1007/s11095-014-1392-5.
20. Reynaud F, Tsapis N, Deyme M, *et al.* Spray-dried chitosan-metal microparticles for ciprofloxacin adsorption: Kinetic and equilibrium studies. Soft Matter. 2011;7:7304–12.
21. Neufeld EF, Muenzer J. The Mucopolysaccharidosis. In: Scriver CR, Beaudet AL, Sly WS, Valle D, editors. The Metabolic and Molecular Bases of Inherited Disease. New York: McGraw-Hill; 2001. p. 3421–52.
22. Giugliani R, Ferderhen A, Carvalho CG, Artigalas O. Enzyme replacement therapy for Mucopolysaccharidosis type I: Laronidase. Pediatr Health. 2010;4:133–45.
23. Souza MV, Krug BC, Picon P, Schwartz IVD. Medicamentos de alto custo para doenças raras no Brasil: o exemplo das doenças lisossômicas. Ciência e Saúde Coletiva. 2010;15(3): 3443–554.
24. Giugliani R, Federhen A, Muñoz Rojas MV, *et al.* Enzyme replacement therapy for mucopolysaccharidoses I, II and VI: recommendations from a group of Brazilian F experts. Rev Assoc Med Bras. 2010;56(3):271–7.
25. Mengual O, Meunier G, Cayre I, Puech K, Snabre P. TURBISCAN MA 2000: multiple light scattering measurement for concentrated emulsion and suspension instability analysis. Talanta. 1999;50(2): 445–56.
26. Mosmann T. Rapid colorimetric assay for cellular growth and survival: application to proliferation and cytotoxicity assays. J Immunol Methods. 1983;65:55–63.
27. Hopwood JJ, Muller V, Smithson A, Baggett N. A fluorometric assay using 4-methylumbelliferyl alpha-L-iduronide for the estimation of alpha-L-iduronidase activity and the detection of Hurler and Scheie syndromes. Clin Chim Acta. 1979;92(2):257–65.
28. Lowry OH, Rosebrough NJ, Farr AL, Randall RJ. Protein measurement with the Folin phenol reagent. J Biol Chem. 1951;193(1):265–75.
29. The European Commission, 2011/696/EU, Official Journal of the European Union, ISSN 1977-0677. 2011;54:L275.
30. Siqueira NM, Contri RV, Paese K, *et al.* Innovative sunscreen formulation based on benzophenone-3-loaded chitosan-coated polymeric nanocapsules. Skin Pharmacol Physiol. 2011;24(3):166–74.
31. Nelson DL, Cox MM. Enzimas. In: Nelson DL, Cox MM, editors. Princípios de bioquímica de Lehninger. São Paulo: Sarvier; 2006. p. 202–12.
32. Celia C, Trapasso E, Cosco D, Paolino D, Fresta M. Turbiscan lab expert analysis of the stability of ethosomes and ultradeformable liposomes containing a bilayer fluidizing agent. Colloids Surf B: Biointerfaces. 2009;72(1):155–60.
33. Ipe BI, Niemeyer CM. Nanohybrids composed of quantum dots and cytochrome P450 as photocatalysts. Angew Chem Int Ed Engl. 2006;45(3):504–7.
34. de Graaf AJ, Kooijman M, Hennink WE, Mastrobattista E. Nonnatural amino acids for site-specific protein conjugation. Bioconjug Chem. 2009;20(7):1281–95.
35. Hong R, Fischer NO, Verma A, *et al.* Control of protein structure and function through surface recognition by tailored nanoparticle scaffolds. J Am Chem Soc. 2004;126(3):739–43.
36. Abad JM, Mertens SF, Pita M, Fernandez VM, Schiffrin DJ. Functionalization of thioctic acid-capped gold nanoparticles for specific immobilization of histidine-tagged proteins. J Am Chem Soc. 2005;127(15):5689–94.
37. Rempel BP, Clarke LA, Withers SG. A homology model for human alpha-l-iduronidase: insights into human disease. Mol Genet Metab. 2005;85(1):28–37.
38. Goldberg M, Langer R, Jia X. Nanostructured materials for applications in drug delivery and tissue engineering. J Biomater Sci Polym Ed. 2007;18(3):241–68.
39. Giugliani R, Rojas VM, Martins AM, *et al.* A dose-optimization trial of laronidase (Aldurazyme) in patients with mucopolysaccharidosis I. Mol Genet Metab. 2009;96(1):13–9.

40. Garnacho C, Dhami R, Simone E, *et al.* Delivery of acid sphingomyelinase in normal and niemann-pick disease mice using intercellular adhesion molecule-1-targeted polymer nanocarriers. J Pharmacol Exp Ther. 2008;325(2):400–8.

41. Hsu J, Serrano D, Bhowmick T, *et al.* Enhanced endothelial delivery and biochemical effects of α-galactosidase by ICAM-1-targeted nanocarriers for Fabry disease. J Control Release. 2011;149:323–31.